

Robust Anisotropic Spin Hall Effect in Rutile RuO₂

Yu-Chun Wang^{1,2}, Zhe-Yu Shen¹, Chia-Hsi Lin¹, Wei-Chih Hsu¹, Yi-Ying Chin³, Akhilesh Kr. Singh⁴, Wei-Li Lee⁴, Ssu-Yen Huang^{1,5&}, and Danru Qu^{2,5*}

¹ *Department of Physics, National Taiwan University, Taipei 10617, Taiwan*

² *Center for Condensed Matter Sciences, National Taiwan University, Taipei 10617, Taiwan*

³ *Department of Physics, National Chung Cheng University, Chia-Yi 621301, Taiwan*

⁴ *Institute of Physics, Academia Sinica, Taipei, 115201, Taiwan*

⁵ *Center of Atomic Initiatives for New Materials, National Taiwan University, Taipei 10617, Taiwan*

& syhuang@phys.ntu.edu.tw (S.Y.H.); * danru@ntu.edu.tw (D.Q.)

Abstract

Altermagnets, which exhibit the advantages of both antiferromagnets and ferromagnets, have attracted significant attention recently. Among them, ruthenium dioxide (RuO₂), a prototypical altermagnet candidate, is under intensive debate on its magnetic order and altermagnetic characters. In this work, we provide a comprehensive study of the spin-to-charge conversion in epitaxial RuO₂ thin films with various orientations and fabrication methods. By utilizing thermal spin injections from a ferrimagnetic insulator, we unambiguously reveal a *negative* spin Hall angle for RuO₂, which is opposite to all the previous reports using ferromagnetic metals. Most importantly, we observe robust anisotropic spin-to-charge conversion in RuO₂, with voltage ratios of 30% for the (100)- and (110)-orientations and 40% for the (101)-orientations. The ratio remains consistent across RuO₂ films fabricated by sputtering, pulsed laser deposition, and molecular-beam epitaxy. These results conclusively show a robust and anisotropic spin Hall effect in RuO₂ with the absence of altermagnetic spin-splitting contributions. Our study provides crucial insights and advances the understanding of spin-to-charge conversions in emerging materials with low crystal symmetries.

Recently, a significant amount of attention has been attracted towards altermagnetism, which is recognized as the third type of magnetism, alongside ferromagnetism and antiferromagnetism [1, 2]. The prominent feature of altermagnetism is that magnetically it is an antiferromagnet with zero net magnetization, therefore beneficial for a faster and robust spintronic device with high device density [3]; While electrically it is similar to a ferromagnet, through the altermagnetic spin-splitting effect (ASSE), it generates a spin-polarized current that efficiently delivers spin angular momentum, allowing the reading and writing of spintronic memory devices. In essence, altermagnets combine the advantages of both antiferromagnets and ferromagnets and hold great potential for spintronic applications.

A prototype altermagnet candidate is ruthenium dioxide (RuO_2) [4]. It has a rutile crystal structure, with space group number 136 ($P4_2/mnm$). It has lattice constant $a = b = 4.5 \text{ \AA}$ and $c = 3.1 \text{ \AA}$. Experiments have shown antiferromagnetic order in RuO_2 through neutron diffraction [5] and resonant x -ray scattering [6], with Néel vectors aligned along the c -axis. The unique crystallographic and magnetic symmetry results in a d -wave-like spin-splitting band in its momentum space [1, 2]. But recent works using muon spin resonance [7], neutron scattering [8] and spin-resolved and angle-resolved photoemission spectroscopy [9] argue that the magnetic order in Ru is absent, posing serious doubt on the altermagnetism in RuO_2 .

Besides the debates on the magnetic order, the reported spin and charge interconversions in RuO_2 [10-16] also face complications. One of the main complications lies in the separation between the spin Hall effect (SHE) and the altermagnetic spin-splitting effect (ASSE) in RuO_2 , which is one of the key features of altermagnetism. Due to the d -wave-like spin-splitting bands in altermagnetic RuO_2 , an *anisotropic* spin and charge interconversion caused by the ASSE or the reciprocal inverse altermagnetic spin-splitting effect (IASSE) is expected. However, the presence of a sizable spin-orbit coupling in RuO_2 and a low crystalline symmetry for the rutile structure

could also result in anisotropy in the SHE or the reciprocal inverse spin Hall effect (ISHE) and thus unavoidably mix the anisotropic ASSE with SHE [16].

Most reported ASSE in RuO_2 are conducted in the (101)-oriented film, which has a low symmetry and a tilted Néel vector away from both the film surface and the surface normal [13-16]. Some studies use the (100)-oriented film, where the Néel vector lies in the film plane [10, 12, 14]. However, both orientations could contain both the anisotropic ASSE and SHE, making the detection of ASSE difficult. To completely isolate the anisotropic SHE, (110)-oriented RuO_2 film is crucial since it does not contain any ASSE at all. However, the study of the (110)-oriented films on cubic substrates like MgO may bring additional extrinsic contributions, such as multi-crystal domains or sample dependence [12, 16], that averages the anisotropic SHE and complex the separation. As a result, the size and sign of both the ASSE and SHE show a large discrepancy among reports [11-16].

Moreover, it is also unclear if different sample preparation methods could induce different impurity levels, which alter the magnetism and thus affect the anisotropic spin-to-charge conversion in RuO_2 . The lack of a comprehensive study on the anisotropic spin Hall effect in rutile RuO_2 impedes our further understanding of the spin-splitting effects. A thorough investigation of the spin-to-charge conversions in epitaxial RuO_2 with different crystal orientations and preparation methods is imperative to resolve these issues.

In this work, we investigate high-quality epitaxial RuO_2 films synthesized by three widely used thin-film deposition techniques: magnetron sputtering, oxide molecular beam epitaxy (oxide MBE), and pulsed laser deposition (PLD). We use three different crystal orientations of TiO_2 substrates, (100)-, (110)-, and (101)-orientations, to enable epitaxial growth of RuO_2 with varied crystal orientations. A capping layer of ferrimagnetic insulator yttrium iron garnet (YIG) is used, serving as the spin current source, and is free from charge current complications. Regardless of

the preparation methods, we obtain a *negative* spin Hall angle for all our RuO₂ films, opposite to Pt and all previous reports on the RuO₂ films. To elucidate this discrepancy, we investigate the electronic structure of Ru in YIG/RuO₂ and permalloy (Py)/RuO₂. The hard *X-ray* photoelectron spectroscopy measurements show the existence of interfacial metal Ru that complicates the spin current transport for the Py/RuO₂ bilayer. Remarkably, with the injected spin being parallel or perpendicular to the *c*-axis or its in-plane projections, we obtain a robust and consistent anisotropic spin-to-charge conversion ratio of 30 % for the (100)- and (110)-RuO₂ and a larger ratio of 40 % for the (101)-RuO₂. These results suggest the absence of the ASSE contribution and a robust anisotropic spin Hall effect in RuO₂.

The RuO₂ layers studied in this work are fabricated under high temperatures of 500 °C using DC sputtering, 350 °C using oxide-MBE, and 650 °C using PLD, and they are denoted as RuO₂^S, RuO₂^M, and RuO₂^P, respectively. X-ray diffraction spectroscopy (XRD) measurements confirm that all the RuO₂ films, regardless of the deposition methods or orientations, have an epitaxial relationship with the TiO₂ substrates [see Supplementary S1]. The YIG layer is deposited by radio-frequency (rf) sputtering at room temperature, followed by rapid thermal annealing in an oxygen atmosphere at 800 °C. X-ray diffraction and magnetization measurements show that after the annealing of YIG, the epitaxial crystallinity of RuO₂ survives, and the YIG layer is crystallized with sizable magnetization [see Supplementary S2]. For comparison, we also prepare a reference Pt sample, deposited onto the epitaxial YIG film grown on the (111)-oriented gadolinium gallium garnet (GGG) substrate [see Supplementary S3], and a reference permalloy (Py) sample, deposited sequentially onto epitaxial RuO₂ film at room temperature.

We first show the conventional spin-to-charge conversion in Pt. Under a vertical temperature gradient of $\nabla T = 13$ K/mm, estimated from an applied heat flux of $Q = 10^5$ W/m² and the YIG thermal conductivity $\kappa = 7.4$ Wm⁻¹K⁻¹, a magnon spin current is excited in a 52-nm-thick YIG due

to the spin Seebeck effect (SSE) [18]. The spin current (J_S) is injected into the 3-nm-thick Pt layer and converted into a transverse charge current (J_C) via the inverse spin Hall effect (ISHE). With a ∇T applied along the $+z$ direction, a magnetic field applied along the $-x$ direction, a sizable and positive thermal voltage V is obtained for Pt, along the $+y$ direction, as shown in Fig. 2(a). We plot our data as a function of the induced electromotive force $E = V/d$, normalized by the distance between the electrodes (d), as shown in Fig. 2(c). The sizable positive saturated electromotive force of $E = 1635$ nV/mm reveals a positive $\theta_{SH} \approx +4\%$ for Pt.

We then illustrate the spin-to-charge conversion in RuO₂ in three commonly used orientations. For the (100)-, (110)-, and (101)-RuO₂, as demonstrated in Fig. 1(a), (d), and (g), a spin current J_S is injected perpendicularly into the films. The injected spin has a spin orientation σ parallel (labeled as σ_1 , as shown in Fig. 1(b), (e), and (h)) or perpendicular (labeled as σ_2 , as shown in Fig. 1(c), (f), and (i)) to c -axis or its in-plane projection. As a result, the induced J_C is expected to contain IASSE for the geometries in Fig. 1(b) and (h), but *not* for the geometries in Fig. 1(c), (e), (f), and (i). In all cases, an ISHE is expected due to the sizable spin-orbit coupling in RuO₂.

To quantitatively study only the inverse spin Hall effect in RuO₂, we first use the (100)-RuO₂, with spin oriented along the $[0\bar{1}0]$ direction, perpendicular to the c -axis, as shown in Fig. 1 (c). Under the spin Seebeck setup, as shown in Fig. 2(b), which is effectively the same as that in Fig. 2(a), a *negative* spin-dependent voltage is observed. Since YIG and TiO₂ are both insulators, the opposite sign in voltage unambiguously reveals a *negative* θ_{SH} for (100)-RuO₂. We observe the negative θ_{SH} also for the MBE fabricated RuO₂^M and PLD fabricated RuO₂^P, and in other crystalline orientations, as shown by the curves in Fig. 3 and 4. The robust and consistent negative θ_{SH} observed in the YIG/RuO₂^{S,M,P}/TiO₂ is against all the positive θ_{SH} observed in [12-16], where ferromagnetic metals, mostly permalloy (Py, Ni₈₀Fe₂₀ alloy), are used as spin current sources or detectors [see Supplementary S4].

We propose two mechanisms to explain the sign discrepancy. Firstly, when a charge current flows in the RuO₂/Py structure for the spin-torque measurements, not only RuO₂ but also Py generates sizable transverse spin current via spin Hall or anomalous Hall effects [17, 18]. We have previously shown that Py has a positive θ_{SH} [17]. However, the existing models on spin current transport in the Py/RuO₂ bilayer overlook these contributions, which could ultimately lead to an overall positive θ_{SH} for the entire RuO₂/Py system. Secondly, Ni₈₀Fe₂₀ (Py) may donate electrons to Ru⁴⁺ in RuO₂ and thus change its valence state. Given that the θ_{SH} for pure Ru film is positive [19], the change of Ru⁴⁺ to a lower valence state can also contribute to a positive θ_{SH} in the Py/RuO₂ bilayer.

This scenario is supported by our hard x-ray photoelectron spectroscopy (HAXPES) measurement on Py/RuO₂, YIG/RuO₂, and RuO₂, sputtered onto (100)-TiO₂ substrates. As shown in Fig. 2(e), upper panel, for the Ru-3d_{5/2} HAXPES spectra, a main peak at 280.8 eV, marked by the black arrow, is observed corresponding to the Ru⁴⁺ state [20-23] for all three samples. However, for Py/RuO₂ spectrum (red), an additional step is observed at around 280 eV, marked by the red arrow, indicating the lower valence state of Ru. The simulated spectra for Py/RuO₂ (middle panel) and YIG/RuO₂ (lower panel) reveal that the step at 280 eV for Py/RuO₂ corresponds to the presence of a Ru metal state [20, 21, 23]. We estimated that around 10 % of Ru⁴⁺ is reduced to the Ru metal state owing to the presence of Py [see Supplementary S5]. Thus, the study using the Py/RuO₂ bilayer is largely affected by the interfacial reduced Ru metal and cannot reflect the true spin-to-charge conversion in RuO₂.

To quantitatively analyze the θ_{SH} of RuO₂, we measure the thickness-dependent ISHE voltage $V_{[001]}$, using the experimental geometry shown in Fig. 2(b). Consistently, a negative θ_{SH} is observed for all our films, ranging from 3.9 nm to 31.6 nm, as shown in Fig. 2(f). Thicker films show smaller voltages due to finite spin diffusion length λ_{sd} , in the scale of a few nanometers,

where spins decay while traversing. We plot the data as a function of thickness, as shown in Fig. 2(g). We fit the results using Eq. 1 in ref [24] and obtain a $\theta_{\text{SH}} = -(4.0 \pm 0.8)\%$ and $\lambda_{\text{sd}} = 1.9 \pm 0.5$ nm [see Supplementary S6 for details].

When the injected spin is aligned along the c -axis for the (100)-RuO₂, as shown in Fig. 1(b), we found $V_{[010]}$ is significantly reduced with a relative $V_{[010]}/V_{[001]}$ of around 30 % [10]. If ASSE plays an important role, the voltage ratio for other crystalline directions, in particular, the (110)-RuO₂, as shown in Fig. 1(d)-(f), which does not contain any ASSE at all, must be sharply different. Surprisingly, we obtain a consistent and robust 30% ratio in the (110)-RuO₂ and 40% in the (101)-RuO₂.

For the YIG/RuO₂^S on (110)-TiO₂ substrate, as shown in Fig. 3(a), the spin current J_S injects into RuO₂^S along the [110] direction, and the detected voltage V_x and V_y are aligned along the [001] and $[\bar{1}10]$ axes, respectively, with spin indices σ oriented along the $[1\bar{1}0]$ and [001] directions. As discussed earlier, both V_x and V_y contain only ISHE and no IASSE. However, the ISHE signal still shows considerable anisotropy with $E_x = -574$ nV/mm and $E_y = -181$ nV/mm, revealing an E_y/E_x ratio of 31 %, as shown in Fig. 3(b). The magnetic field (H) angular-dependent measurements of E_x and E_y , with H rotated in the xy plane, with angle ϕ respect to the x -axis, as shown in Fig. 3(c), are nicely fit using the cosine and sine curves, respectively.

For the YIG/RuO₂^S/TiO₂ (101) sample, as shown in Fig. 3(d), the pure spin current J_S flows into the film along the film's normal direction. The detected voltages V_x and V_y are aligned along the $[\bar{1}01]$ and [010] directions, respectively. The corresponding spin indices σ are oriented along $[0\bar{1}0]$ and $[\bar{1}01]$ axes. For E_x , σ is perpendicular to c -axis, with solely ISHE and no ASSE contribution. For E_y , σ is parallel to the in-plane projection of c -axis, thus containing partial ISHE and IASSE contributions. As shown in Fig. 3(d), we obtain $E_x = -677$ nV/mm and $E_y = -253$ nV/mm, yielding an E_x/E_y ratio of 38 %. The magnetic field (H) angular-dependent measurements

of E_x and E_y , with H rotated in the xy plane, as shown in Fig. 3(f), are also fit nicely by the cosine and sine dependence, respectively.

Here, we use the anisotropic spin Hall effect to understand our experimental observation. Since the space group for RuO₂ is No. 136 (P4₂/mnm), it has three independent spin Hall conductivity $\sigma_{ab}^c \neq \sigma_{bc}^a \neq \sigma_{ca}^b$ [25], where a , b , and c represent the [100] -, [010] -, and [001]-axes, respectively. According to [16] and [Supplementary S6], we assign A , B , and C as the spin Hall conductivity $\sigma_{ab}^c = -\sigma_{ba}^c = A$, $\sigma_{bc}^a = -\sigma_{ac}^b = B$, and $\sigma_{ca}^b = -\sigma_{cb}^a = C$. The altermagnetic spin-splitting conductivity is denoted as σ_{IASSE} , representing the transverse charge-to-spin conversion via the spin-splitting effect. Through the transformation matrix, we calculate $E_y/E_x = (A + \sigma_{\text{IASSE}})/B$ for (100)-RuO₂; $E_y/E_x = A/B$ for (110)-RuO₂; and $E_y/E_x = (0.32A + 0.68C + 0.32\sigma_{\text{IASSE}}) / (0.68C + 0.32B)$ for (101)-RuO₂. The consistent 30% E_y/E_x ratio for (100)- and (110)-RuO₂ leads to $(A + \sigma_{\text{IASSE}})/B \approx A/B \approx 30\%$, which suggests a striking result of $\sigma_{\text{IASSE}} \sim 0$. The result indicates that the altermagnetic spin-splitting contribution is negligible, while the spin Seebeck voltage anisotropy is solely caused by the spin Hall effect anisotropy. On the other hand, for the (101)-RuO₂, the larger E_y/E_x of 38% reveals $C/B = 8\%$. Considering the spin Hall angle for the (100)-RuO₂ as -4.0% and the estimated resistivity for the bulk RuO₂ as 157 $\mu\Omega\text{cm}$ [see Supplementary S4], we obtain the anisotropic spin Hall angle and conductivity for each orientation as $\theta_{SH_{bc}}^a \approx -(4.0 \pm 0.8)\%$, $\theta_{SH_{ca}}^b \approx -(0.3 \pm 0.06)\%$, $\theta_{SH_{ab}}^c \approx -(1.2 \pm 0.2)\%$, $\sigma_{bc}^a \approx -250 \pm 51 \text{ Scm}^{-1}$, $\sigma_{ca}^b \approx -19 \pm 3 \text{ Scm}^{-1}$, and $\sigma_{ab}^c \approx -75 \pm 15 \text{ Scm}^{-1}$. These results are summarized in Table I.

To show the independence of the fabrication methods, we also study the anisotropic spin-to-charge conversion in the MBE and PLD fabricated RuO₂ film epitaxially grown on TiO₂. As shown in Fig. 4 (a) and (b), we consistently observe an anisotropy in the spin-to-charge conversion. The ratios of E_y (perpendicular to the c -axis) to E_x (parallel to the c -axis) in these RuO₂ films remain

impressively at 30 % for (100)- and (110)-orientation and 40 % for the (101)-orientation. The orientation dependence based on 15 samples studied in the work is summarized in Fig. 4(c), where the E_y/E_x ratio for (100)-, (110)-, and (101)-orientations are 31.9 ± 5.6 %, 28.4 ± 4.1 %, and 38.9 ± 5.2 %, respectively. The consistency among samples prepared by different methods shows the robustness of the anisotropic spin Hall effect in RuO₂. These results also provide critical insight into the study of the anisotropic spin Hall effect for other altermagnet candidates with low crystalline symmetry. We also point out that, unlike many studies that report anisotropy using different samples, the anisotropy ratios for RuO₂ obtained in this work are based on the anisotropic spin Hall effect within the *same* samples. For example, we obtain A/B using the (100)-RuO₂ and C/B using the (101)-RuO₂ sample. Although the absolute value of A , B , and C may have sample dependence, the ratio remains consistent and intrinsic, regardless of the preparation methods.

In conclusion, we have comprehensively studied the spin-to-charge conversion in RuO₂ thin films with varying crystal orientations and fabrication methods. Our results consistently show a negative spin Hall angle across all the epitaxial RuO₂ films studied in this work, as determined through thermal spin current injection from the ferromagnetic insulator YIG. The HAXPES measurements reveal the presence of interfacial metal Ru, which may influence spin current transport in the Py/RuO₂ bilayer. From thickness-dependent measurements, we extract both the spin Hall angle and spin diffusion length. Most importantly, we observe a robust and consistent anisotropic spin Hall effect in RuO₂ with an E_y/E_x ratio of 30% for the (100)- and (110)-oriented RuO₂ and 40% for the (101)-oriented RuO₂. This anisotropy remains unchanged across RuO₂ fabricated via sputtering, MBE, and PLD. These results suggest a minimal contribution from the altermagnetic spin-splitting effect and a dominant role of the anisotropic spin Hall effect in the rutile RuO₂. Our findings provide valuable insights into spin-charge interconversion mechanisms in RuO₂ and other altermagnetic candidates with low crystalline symmetry.

Acknowledgment

This work at NTU has been supported by the National Science and Technology Council under Grant No. NSTC 113-2628-M-002-019, NSTC 112-2123-M-002-001, NSTC 113-2112-M-002-039, NSTC 113-2112-M-194-002, and NSTC 113-2124-M-001-011. Center of Atomic Initiative for New Materials (AI-MAT), National Taiwan University, within the Higher Education Sprout Project by the Ministry of Education in Taiwan.

Spin Hall Angle	$\theta_{SH_{bc}}^a$	$\theta_{SH_{ca}}^b$	$\theta_{SH_{ab}}^c$
(%)	-4.0 ± 0.8	-0.3 ± 0.06	-1.2 ± 0.2
Spin Hall Conductivity	$\sigma_{bc}^a = -\sigma_{ac}^b$	$\sigma_{ca}^b = -\sigma_{cb}^a$	$\sigma_{ab}^c = -\sigma_{ba}^c$
($S\text{cm}^{-1}$)	-250 ± 51	-19 ± 3	-75 ± 15
Anisotropy Ratio	$\sigma_{bc}^a/\sigma_{bc}^a$	$\sigma_{ca}^b/\sigma_{bc}^a$	$\sigma_{ab}^c/\sigma_{bc}^a$
(%)	100	8	30

Table I. Summarization of the anisotropic spin Hall angle, spin Hall conductivity, and anisotropy ratio obtained from the anisotropic spin-to-charge conversion in RuO₂.

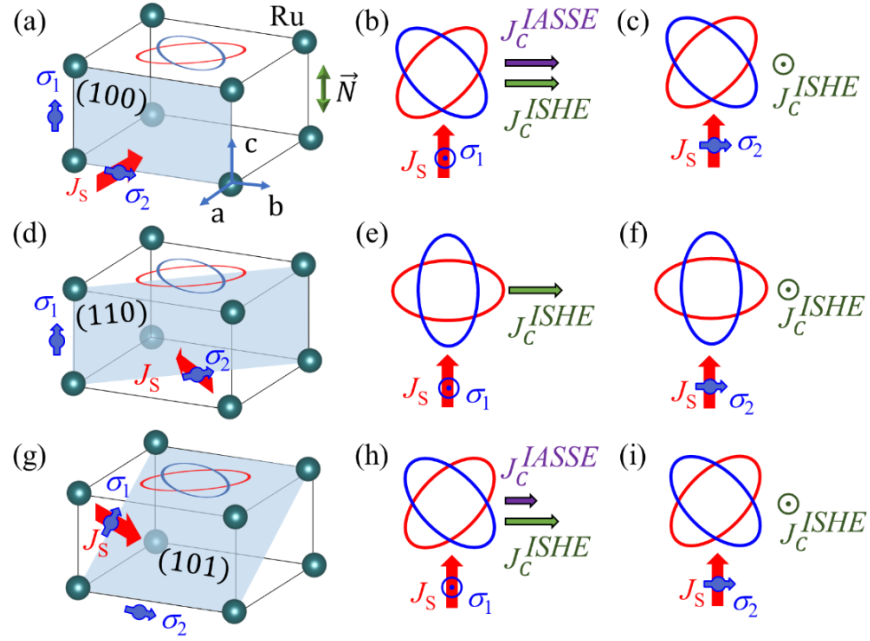


FIG. 1. Schematic illustrations of the rutile-RuO₂ crystal structure, highlighting (a) the (100)-plane, (d) the (110)-plane, and (g) the (101)-plane. Schematic illustrations of the d -wave spin-splitting band with injected spin oriented (b), (e), (h) parallel or (c), (f), (i) perpendicular to c -axis or its in-plane projection. In all cases, ISHE are expected, while only (b) and (h) generate IASSE.

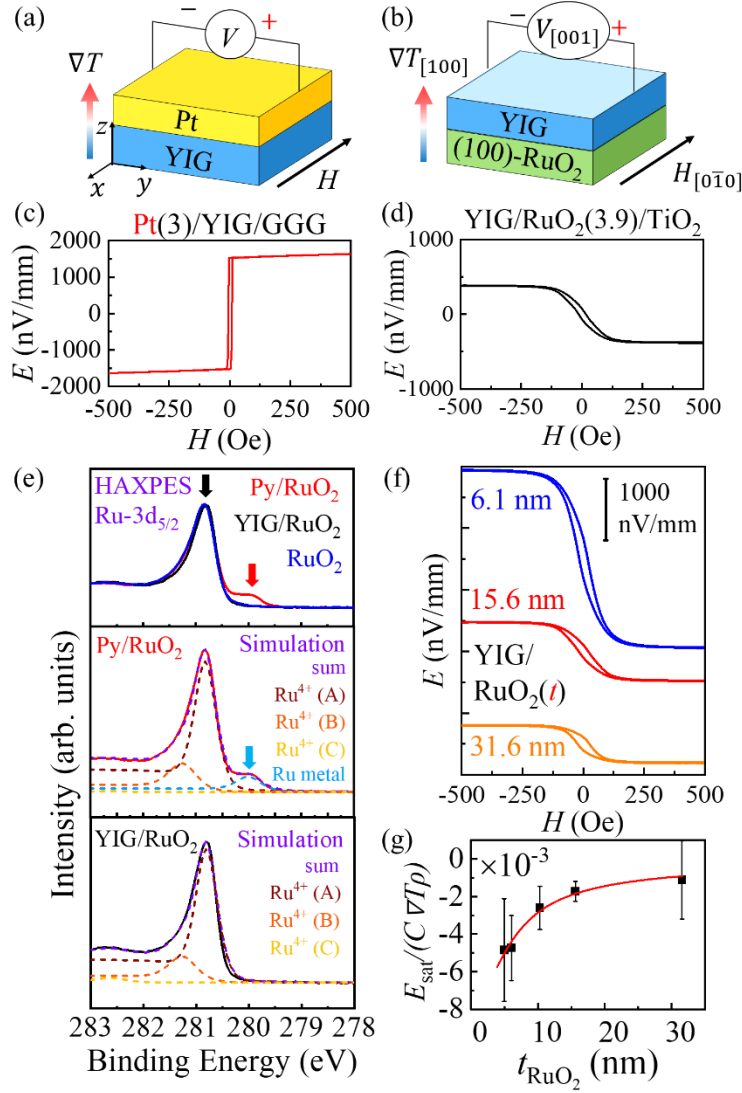


FIG. 2. Schematic illustrations of spin Seebeck measurements for (a) Pt/YIG/GGG and (b) YIG/RuO₂/TiO₂. The spin current injection direction follows the temperature gradient and thus is the same for (a) and (b), regardless of YIG layer sequence. The spin Seebeck voltages for (c) Pt (3 nm)/YIG grown on (111)-oriented and (d) YIG/RuO₂ (3.9 nm). (e) HAXPES spectra (top panel) and simulations (middle and bottom panels) for Py/RuO₂ (red), YIG/RuO₂ (black), and RuO₂ (blue). Thickness dependent (f) spin Seebeck electromotive force and (g) normalized plot for RuO₂ of various thicknesses. All these RuO₂ films are sputtered onto the (100)-oriented TiO₂ substrate.

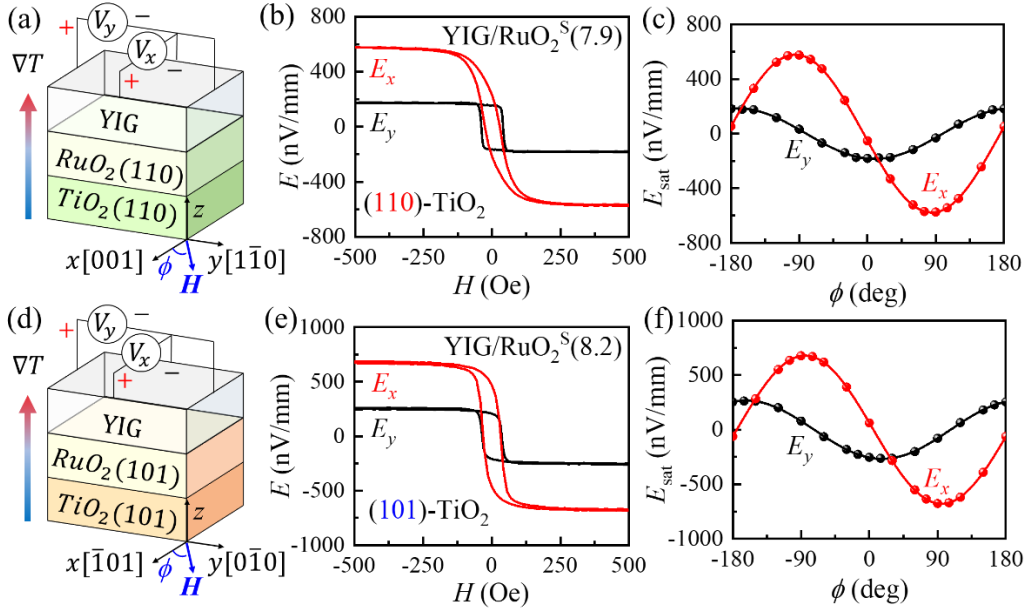


FIG. 3. Schematic illustrations of experiment setup for (a) (110)-oriented and (d) (101)-oriented YIG/RuO₂/TiO₂ samples. The x -axis is aligned parallel to the [001]- and the $[\bar{1}01]$ -axis in (a) and (d), respectively. ϕ represents the angle between the external magnetic field and the x -axis. The spin Seebeck voltage and the H -angular-dependence is obtained for (b)-(c) (110)-RuO₂^S and (d)-(f) (101)-RuO₂^S, respectively.

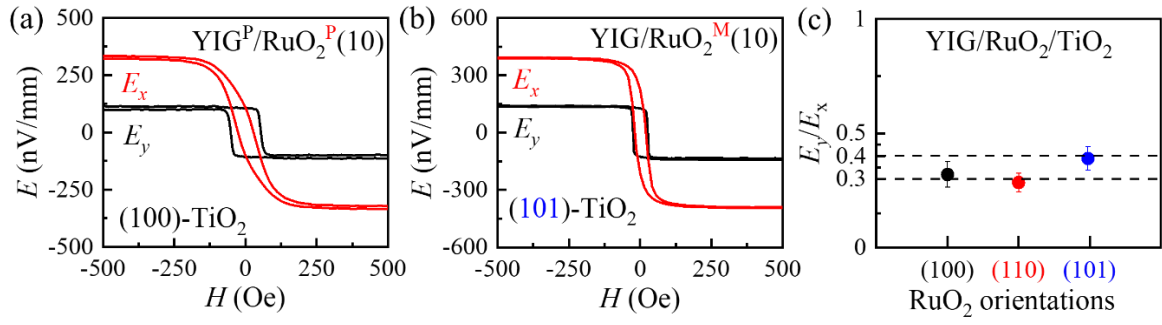


Fig. 4. Anisotropic spin Seebeck voltages for (a) PLD-fabricated and (b) MBE-fabricated RuO₂.
(c) Summarization of orientation-dependent E_y/E_x ratios for all samples studied in this work.

References:

1. L. Šmejkal, J. Sinova, and T. Jungwirth, Beyond Conventional Ferromagnetism and Antiferromagnetism: A Phase with Nonrelativistic Spin and Crystal Rotation Symmetry, *Phys. Rev. X* **12**, 031042 (2022).
2. L. Šmejkal, J. Sinova, and T. Jungwirth, Emerging Research Landscape of Altermagnetism, *Phys. Rev. X* **12**, 040501 (2022).
3. V. Baltz, A. Manchon, M. Tsoi, T. Moriyama, T. Ono, and Y. Tserkovnyak, Antiferromagnetic spintronics, *Rev. Mod. Phys.* **90**, 015005 (2018).
4. L. Šmejkal, R. González-Hernández, T. Jungwirth, and J. Sinova, Crystal time-reversal symmetry breaking and spontaneous Hall effect in collinear antiferromagnets, *Sci. Adv.* **6**, eaaz8809 (2020).
5. T. Berlijn, P. C. Snijders, O. Delaire, H.-D. Zhou, T. A. Maier, H.-B. Cao, S.-X. Chi, M. Matsuda, Y. Wang, M.R. Koehler, P.R.C. Kent, and H. H. Weitering, Itinerant Antiferromagnetism in RuO₂, *Phys. Rev. Lett.* **118**, 077201 (2017).
6. Z. H. Zhu, J. Stremper, R. R. Rao, C. A. Occhialini, J. Pelliciari, Y. Choi, T. Kawaguchi, H. You, J.F. Mitchell, Y. Shao-Horn, and R. Comin, Anomalous Antiferromagnetism in Metallic RuO₂ Determined by Resonant X-ray Scattering, *Phys. Rev. Lett.* **122**, 017202 (2019).
7. M. Hiraishi, H. Okabe, A. Koda, R. Kadono, T. Muroi, D. Hirai, and Z. Hiroi, Nonmagnetic Ground State in RuO₂ Revealed by Muon Spin Rotation, *Phys. Rev. Lett.* **132**, 166702 (2024).
8. P. Keßler, L. Garcia-Gassull, A. Suter, T. Prokscha, Z. Salman, D. Khalyavin, P. Manuel, F. Orlandi, I. I. Mazin, R. Valentí, and S. Moser, Absence of magnetic order in RuO₂: insights from μ SR spectroscopy and neutron diffraction, *npj Spintronics* **2**, 50 (2024).
9. J. Liu, J. Zhan, T. Li, J. Liu, S. Cheng, Y. Shi, L. Deng, M. Zhang, C. Li, J. Ding, Q. Jiang, M. Ye, Z. Liu, Z. Jiang, S. Wang, Q. Li, Y. Xie, Y. Wang, S. Qiao, J. Wen, Y. Sun, and D. Shen, Absence of Altermagnetic Spin Splitting Character in Rutile Oxide RuO₂, *Phys. Rev. Lett.* **133**, 176401 (2024).
10. C.-T. Liao, Y.-C. Wang, Y.-C. Tien, S.-Y. Huang, and D. Qu, Separation of Inverse Altermagnetic Spin-Splitting Effect from Inverse Spin Hall Effect in RuO₂, *Phys. Rev. Lett.* **133**, 056701 (2024).
11. H. Bai, Y. C. Zhang, Y. J. Zhou, P. Chen, C. H. Wan, L. Han, W. X. Zhu, S. X. Liang, Y. C. Su, X. F. Han, F. Pan, and C. Song, Efficient Spin-to-Charge Conversion via Altermagnetic Spin Splitting Effect in Antiferromagnet RuO₂, *Phys. Rev. Lett.* **130**, 216701 (2023).
12. H. Bai, L. Han, X. Y. Feng, Y. J. Zhou, R. X. Su, Q. Wang, L. Y. Liao, W. X. Zhu, X. Z. Chen, F. Pan, X. L. Fan, and C. Song, Observation of Spin Splitting Torque in a Collinear Antiferromagnet RuO₂, *Phys. Rev. Lett.* **128**, 197202 (2022).
13. A. Bose, N. J. Schreiber, R. Jain, D.-F. Shao, H. P. Nair, J. Sun, X. S. Zhang, D. A. Muller, E. Y. Tsymbal, D. G. Schlom and D. C. Ralph, Tilted spin current generated by the collinear antiferromagnet ruthenium dioxide, *Nature Electronics* **5**, 267 (2022).
14. S. Karube, T. Tanaka, D. Sugawara, N. Kadoguchi, M. Kohda, and J. Nitta, Observation of Spin-Splitter Torque in Collinear Antiferromagnetic RuO₂, *Phys. Rev. Lett.* **129**, 137201 (2022).
15. Y. Fan, Q. Wang, W. Wang, D. Wang, Q. Huang, Z. Wang, X. Han, Y. Chen, L. Bai, S. Yan, and Y. Tian, Robust Magnetic-Field-Free Perpendicular Magnetization Switching by Manipulating Spin Polarization Direction in RuO₂/[Pt/Co/Pt] Heterojunctions, *ACS Nano* **18**, 26350 (2024).

16. Z. Q. Wang, Z. Q. Li, L. Sun, Z. Y. Zhang, K. He, H. Niu, J. Cheng, M. Yang, X. Yang, G. Chen, Z. Yuan, H.F. Ding, and B.F. Miao, Inverse Spin Hall Effect Dominated Spin-Charge Conversion in (101) and (110)-Oriented RuO₂ Films, *Phys. Rev. Lett.* **133**, 046701 (2024).
17. B. F. Miao, S. Y. Huang, D. Qu, and C. L. Chien, Inverse Spin Hall Effect in a Ferromagnetic Metal, *Phys. Rev. Lett.* **111**, 066602 (2013).
18. Y. Yang, Z. Luo, H. Wu, Y. Xu, R.-W. Li, S. J. Pennycook, S. Zhang, and Y. Wu, Anomalous Hall magnetoresistance in a ferromagnet, *Nat. Comm.* **9**, 2255 (2018).
19. Z. Wen, J. Kim, H. Sukegawa, M. Hayashi, and S. Mitani, Spin-orbit torque in Cr/CoFeAl/MgO and Ru/CoFeAl/MgO epitaxial magnetic heterostructures, *AIP Advances* **6**, 056307 (2016).
20. C. L. Bianchi, V. Ragaini, and M. G. Cattania, An XPS study on ruthenium compounds and catalysts, *Mater. Chem. Phys.* **29**, 297-306 (1991).
21. Y. Kaga, Y. Abe, H. Yanagisawa, M. Kawamura, and K. Sasaki, Ru and RuO₂ Thin Films by XPS, *Surf. Sci. Spectra* **6**, 68 (1999).
22. C. D. Wagner, A. V. Naumkin, A. Kraut-Vass, J. W. Allison, C. J. Powell, J. R. Rumble, in *NIST X-ray Photoelectron Spectroscopy Database, Version 4.1*, National Institute of Standards and Technology, Gaithersburg, 2012.
23. D. J. Morgan, Resolving ruthenium: XPS studies of common ruthenium materials, *Surf. Interface Anal.* **47**, 1072–1079 (2015).
24. D. Qu, T. Higo, T. Nishikawa, K. Matsumoto, K. Kondou, D. Nishio-Hamane, R. Ishii, P. K. Muduli, Y. Otani, and S. Nakatsuji, Large enhancement of the spin Hall effect in Mn metal by Sn doping, *Phys. Rev. Mater.* **2**, 102001(R) (2018).
25. A. Roy, M. H. D. Guimarães, and J. Sławińska, Unconventional spin Hall effects in nonmagnetic solids, *Phys. Rev. Mater.* **6**, 045004 (2022).